Taylor & Francis
Taylor & Francis Group

MINI-REVIEW

Principles, Instrumentation, and Applications of Infrared Multispectral Imaging, An Overview

Chieu D. Tran

Department of Chemistry, Marquette University, Milwaukee, Wisconsin

Abstract: An infrared (IR) multispectral imaging spectrometer is an instrument that can simultaneously record infrared spectroscopic and spatial information of a sample. Chemical and physical properties of the sample can be elucidated from such images. In a multispectral imaging instrument, a camera is used to record the spatial distribution of the sample, and the spectral information is obtained with a dispersive device. This overview article describes operational principles and recent development of various components used in IR multispectral imaging instruments, including the electronic dispersive devices (acousto-optic tunable filter and liquid crystal tunable filter) and near- and middle-IR cameras (InGaAs, InSb, HgCdTe, and QWIP cameras). Recent applications and unique use of the IR imaging instruments will be described followed by discussion of the future prospects of the technique.

Keywords: Acousto-optic tunable filter, acousto-optic tunable filter, liquid crystal tunable filter, focal plane arrays, In-Ga-As, InSb, HgCdTe, infrared, imaging

INTRODUCTION

Infrared (IR) multispectral imaging, sometimes referred to in literature as spectroscopic imaging, hyperspectral imaging, or chemical imaging, is a relatively new technique that combines spectroscopy and imaging, namely, it records the chemically rich information available from spectroscopy in a

spatially resolved manner (Morris 1993). In this instrument, the recorded images contain signals that are generated by molecules or units in a sample, plotted as a function of spectral and spatial distribution (Morris 1993). As such, a single data set consists of both spatial and spectral information. The typical dimensions of this data set range from 256×256 to 1024×1024 pixels, with each pixel containing a full IR spectrum. Such data will facilitate visualizing chemical distribution in a sample or chemical compositions of several samples. This type of information is of particular importance, as it is known that chemical as well as physical properties of materials are dependent on the chemical distribution within the samples. Instrumentally, in a multispectral imaging instrument, an infrared camera is used to record the spatial distribution of the sample, and the spectral information is obtained by scanning a dispersive device to record spectra for each image (Morris 1993). Dispersive devices based on mechanical scanning (e.g., filter wheels, monochromators) are not desirable, because they have relatively large size (and, hence, are impractical for field deployment), are prone to vibrations, and can only be spectrally tuned in a relatively narrow range with a relatively slow speed. Recent advances in material sciences, electronics, and computer sciences have led to the development of novel types of electronically tunable filters. Acousto-optic tunable filters (AOTFs) (Tran and Bartelt 1992; Tran and Simianu 1992; Tran and Furlan 1992a; 1992b, 1993, 1994; Tran 1992, 1995, 1997, 2000a; Tran, Furlan, and Lu 1994; Tran and Lu 1995, 1996; Pasquini et al. 1996; Baptista, Tran, and Gao 1996; Tran and Gao 1996, 1997; Alexander, Gao, and Tran 1997; Tran and Huang 1999) and liquid crystal tunable filters (LCTFs) (Miller 1991, 1995) belong to these types of electronic tuning devices. They are particularly suited for use in multispectral imaging instruments, as they contain no moving parts and can be spectrally tuned over a wide spectral range (from near-IR to middle-IR) with much faster speeds (from micro- to milliseconds).

Development in material science, optics, and electronics have made high-performance and high-sensitivity cooled and uncooled infrared array detectors (also known as IR focal plance arrays [FPAs]) available at relatively reasonable costs. FPAs based on various materials (InGaAs, InSb, HgCdTe, and QWIP) with different numbers of pixels (from 64×64 to 1024×1024 pixels) and different spectral detection ranges (from $1\,\mu m$ to $12\,\mu m$) are now readily commercially available (Cohen and Olsen 1993; Barton, Cannata, and Petronio 2002; Kozlowski et al. 1997; Kimata 1998; Rogalski 2001; Kozlowski 1997; Gopal 1998; Faraone 1998; Gunapal et al. 2001).

Various types of IR multispectral imaging instruments have been developed in recent years. These instruments made it possible to perform studies and measurements that, to date, were not possible otherwise. In this overview, detailed information on operation principles and advantages and disadvantages of various types of electronic tuning devices (AOTFs and LCTFs) and infrared cameras (InGaAs, InSb, HgCdTe, and QWIP focal

plane arrays) will be described. Comparison of different near- and middle-IR multispectral imaging systems will be made, including some of their unique applications. It is noteworthy to add that this overview covers only multispectral imaging systems based on tunable filters, namely, AOTFs and LCTFs. The Fourier-transform (FT) technique based on Michelson interferometer can also be used as a dispersive device in multispectral imaging instruments. In fact, multispectral imaging instruments based on FT-Michelson interferometer have been developed (Lewis et al. 1995, 1997; Snively et al. 1999; Weerd et al. 2002; Rafferty et al. 2002; Scott, Bhargava, and Levin 2002; Colarusso et al. 1998; Bhargava and Levin 2001) and are commercially available from several manufacturers. Multispectral imaging based on FT will not be covered in this overview, because not only is spectral tuning mechanism for the FT distinctly different from those of the AOTFs and LCTFs, but also it has been the subject of several reviews (Colarusso et al. 1998; Bhargava and Levin 2001). The last part of this mini-review will be focused on recent analytical applications of AOTF- or LCTF-based IR multispectral imaging instruments.

INSTRUMENTATION

Spectral Tuning Devices

Acousto-Optic Tunable Filters

Theory and operational principles of an acousto-optic tunable filter (AOTF) have been described in detail in some recent reviews (Tran 1992, 1997, 2000a). Essentially, AOTF is an all-solid-state, electronic dispersive device based on the principle of a collinear (longitudinal) interaction between an ordinary ray (o-ray), an extraordinary ray (e-ray), and a traveling acoustic wave in a birefringent crystal. Generally, the AOTF is constructed from a birefringent crystal onto which an array of $LiNbO_3$ piezoelectric transducers is bonded. A radio frequency (RF) signal is applied to the transducers that, in turn, generate, acoustic waves propagating through the crystal. These propagating acoustic waves produce a periodic moving grating that will diffract portions of an incident light beam. Under certain conditions, a light beam propagating as an e-ray can, under some conditions, be converted into an o-ray and, in addition, be spatially separated from the original e-ray by interaction with, and diffraction from, an acoustic wave propagating in the same medium. The phase-matching condition (i.e., conservation of momentum) must be satisfied in order for this conversion to be cumulative. As a consequence of this conservation of momentum, for a fixed acoustic frequency and sufficient long interaction length, only a very narrow band of optical frequencies can approximately satisfy the phase-matching condition and be

diffracted. The (narrow) spectral bandpass of the filter can, therefore, be tuned over large optical regions by simply changing the frequency of the applied rf signal. The wavelength of the diffracted light (λ_o) is related to the frequency of the acoustic wave (f_a) by the following condition:

$$f_a = [\nu_s(n_i - n_d)]\frac{1}{\lambda_o}(\sin^4\theta_i + \sin^2 2\theta_i)^{1/2} \qquad (1)$$

As depicted in Equation (1), for a fixed acoustic frequency and sufficiently long interaction length, only a very narrow band of optical frequencies can approximately satisfy the phase-matching condition and be diffracted. The wavelength of the diffracted light can, therefore, be tuned over large spectral regions by simply changing the frequency of the applied RF signal. Figure 1 shows the spectral tuning curse of a noncollinear AOTF fabricated from TeO_2 for the NIR region. As illustrated, light can be spectrally tuned from 1.1 μm to 2.4 μm by simply scanning the frequency of the applied RF signal from 60 MHz to 30 MHz (Tran and Bartelt 1992; Tran and Simianu 1992; Tran and Furlan 1992a, 1992b, 1993, 1994; Tran 1992, 1995, 1997, 2000a; Tran, Furlan, and Lu 1994; Tran and Lu 1995, 1996; Pasquini et al. 1996; Baptista, Tran, and Gao 1996; Tran and Gao 1996, 1997; Alexander, Gao, and Tran 1997; Tran and Huang 1999).

Depending on the spectral region, different birefringent crystals are used to fabricate AOTFs. Three most widely used crystals for AOTFs are shown in Table 1. Quartz is often used for AOTF in the ultraviolet (UV) and visible region (Tran and Lu 1995). Quartz is known to have relatively good optical transparency for UV and visible region. However, because it has a relatively low acoustic figure of merit (ability to allow acoustic waves to be applied to the crystal), AOTFs based on quartz often require, in addition to collinear
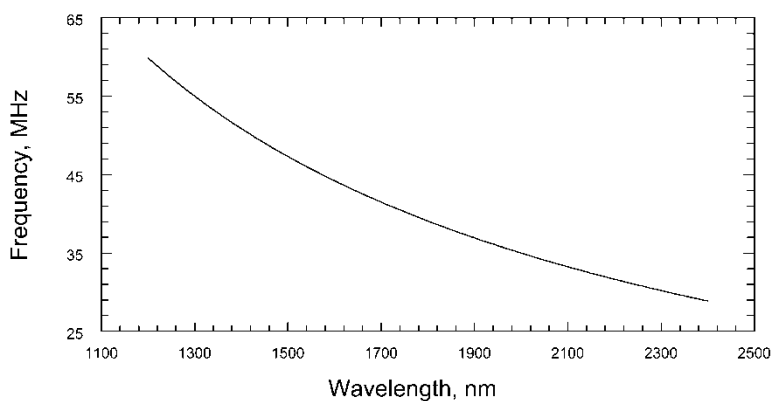

Figure 1. Typical spectral tuning curve of a noncollinear TeO_2 AOTF for the near-infrared region.

Table 1. Properties of widely used crystals to fabricate AOTFs

Material	Transparency range (μm)	Acoustic figure of merit
Quartz	0.2–4.5	1
TeO$_2$	0.35–5.0	795
Tl$_3$AsSe$_3$	1.0–16	900

configuration (in order to enhance acousto-optic interaction length l), relatively high power of applied RF signal. The high RF power consumption somewhat limits applications of the quartz-based AOTFs (Tran and Lu 1995). Furthermore, the collinear configuration renders this type of AOTF difficult to use in multispectral imaging instruments, because the transmitted (undiffracted) light is spatially in the same direction as the diffracted light, thereby making removal of the unfiltered, undiffracted light difficult. Different from quartz, TeO$_2$ crystal is suitable for AOTF from the visible region (from about 340 nm) to the infrared or about 5 μm, where it becomes opaque. Tl$_3$AsSe$_3$ (often known as TAS) can be used for AOTF from 1 to 16 μm. Because these two crystals have relatively higher acoustic figures of merit (795-fold and 900-fold higher than quartz), AOTFs based on these crystals require relatively lower power of applied RF and signal. It addition, they can be constructed using noncollinear configuration (Tran and Bartelt 1992; Tran and Simianu 1992; Tran and Furlan 1992a, 1992b, 1993, 1994; Tran 1992, 1995, 1997, 2000a; Tran, Furlan, and Lu 1994; Tran and Lu 1995, 1996; Pasquini et al. 1996; Baptista, Tran, and Gao 1996; Tran and Gao 1996, 1997; Alexander, Gao, and Tran 1997; Tran and Huang 1999). As a consequence, TeO$_2$- and Tl$_3$AsSe$_3$-based AOTFs are particularly suited and most often are filter of choice for use in multispectral imaging instruments.

Of particular importance to the multispectral imaging technique is the scanning speed of the AOTF. The scanning speed of the filter is defined by the speed of the acoustic wave in the crystal, which is on the order of microseconds (Tran and Bartelt 1992; Tran and Simianu 1992; Tran and Furlan 1992a, 1992b, 1993, 1994; Tran 1992, 1995, 1997, 2000a; Tran, Furlan, and Lu 1994; Tran and Lu 1995, 1996; Pasquini et al. 1996; Baptista, Tran, and Gao 1996; Tran and Gao 1996, 1997; Alexander, Gao, and Tran 1997, Tran and Huang 1999). As a consequence, AOTFs have the fastest scanning speeds compared to other dispersive devices, including conventional gratings, LCTFs, and interferometers.

Taken together, the AOTFs offer such advantages as being compact, being all-solid state (contains no moving parts), having rapid scanning ability (microseconds), having wide spectral tuning range (from visible to

NIR and IR), and having high throughput (>90% diffraction efficiency for incident polarized light), allowing high-speed random or sequential wavelength access and giving high resolution (a few angstroms). As a consequence, AOTFs are particularly suited for use as dispersive devices in a multispectral imaging instrument. In fact, AOTF-based multispectral imaging spectrometers have been developed for the near- and middle-IR. A schematic diagram of such on instrument is shown in Figure 2 (Tran, Cui, and Smirnov 1998; Fischer and Tran 1999a, 1999b; Tran 2000b, 2001; Khait, Smirnov, and Tran 2000, 2001; Alexander and Tran 2001a, 2001b; Politi, and Tran 2002).

Liquid-Crystal Tunable Filters

A liquid-crystal tunable filter is a notch filter with a center wavelength that can be varied (tuned) by changing the applied voltage (Miller 1991, 1995). This type of notch filter is known as a "Lyot filter." In a Lyot filter, a birefringent crystal is placed between two polarizers with axes that are parallel to each other. The input polarizer converts incoming unpolarized light into linearly polarized light. The polarized light then passes through the birefringent crystal, where it is split into ordinary and extraordinary beams. The birefringent crystal also introduces phase delay between the two beams (and hence, it is called a retarder). The optical path difference between the two beams is known as a retardance Γ. For light with wavelength λ, the phase
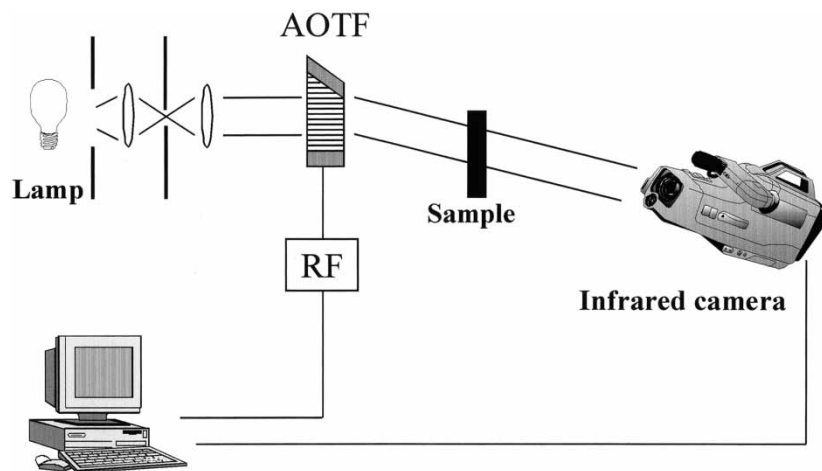

Figure 2. The infrared multispectral imaging instrument based on an acousto-optic tunable filter: AOTF, acousto-optic tunable fitler; RF, RF signal generator.

difference δ is introduced by a retarder, with a retardance Γ given by the following (Miller 1991, 1995):

$$\delta = \frac{2\pi\Gamma}{\lambda} \qquad (2)$$

The light coming out of the retarder then passes through a second polarizer (known as an analyzer). The intensity of the transmitted beam is dependent on $\cos^2\delta$. As a consequence, only light with certain wavelength can be transmitted. Specifically, light with wavelength for which $\Gamma = k\lambda$ will experience high transmittance, while those for which $\Gamma = (k+1)\lambda$ will be extinguished. Generally, a Lyot filter is constructed by placing each quartz or calcite birefringent retarder in series with a liquid-crystal variable waveplate. The liquid-crystal waveplate is essentially an electrically variable retardance that provides the means to spectrally tune the filter. The retardance of stage i is given by the following (Miller 1991, 1995):

$$\Gamma = 2^i\lambda \qquad (3)$$

Light of wavelength λ is transmitted without loss, because it meets the transmission criteria for each stage, while light of other wavelengths is extinguished by one or more stages.

A variety of factors including limited availability of materials that possess electro-optic properties and materials that can be used to construct thin but high extinction ratio polarizers, LCTFs, which are currently available, can only be tuned to an upper limit wavelength of 1700 nm. Furthermore, because of properties of electro-optic materials and the characteristics of the Lyot filters, the spectral tuning range of this type of filter is relatively narrower than those of the AOTFs. Typically, a NIR LCTF can be spectrally tuned from 1000 to 1700 nm. However, the narrow spectral tuning range of the LCTFs should not restrict their applications in multispectral imaging instruments. This is because this tuning range (1000–1700 nm) matches well with the InGaAs focal plane arrays cameras for the NIR region. In addition, LCTFs have relatively large acceptance angles and are commercially available with relatively larger apertures than AOTFs. (NIR LCTFs are available with aperture as large as 20 mm). Because these features can somewhat compensate for the relatively lower transmission efficiencies of the LCTFs, the LCTFs can be used for the construction of multispectral imaging instruments. In fact, multispectral imaging instruments based on LCTFs have been constructed and used for various types of important studies (Morris, Schaeberle, and Treado 1995; Turner and Treado 1997). However, compared to AOTF-based multispectral imaging instruments, LCTF-based instruments cannot be used for measurements that require fast scanning speed. This is due to the fact that while the AOTFs can be spectrally scanned in microseconds, the fastest speed at which LCTF can be tuned is

only milliseconds. The slower speed of the LCTFs is due to the slower electro-optical responses of the materials used to construct the filters.

Infrared Focal Plane Arrays

In principle, it is possible to record multispectral images with single-point detectors (by translating the sample in the X and Y directions). However, array detectors that can simultaneously measure light with multiple detector elements are often required, as they can significantly reduce recording time and provide uniformed background and high S/N ratio. High-performance array detectors for the UV and visible region (charge coupled devices [CCD] and complementary metal oxide semiconductor [CMOS]) are readily commercially available with low background, high sensitivity at relatively low cost, because they are based on mature technology. Conversely, IR array detectors or IR cameras (also known as IR FPAs) were originally developed for military applications and surveillance and have only become commercially available recently. Furthermore, they are based on technology that is relatively less developed than that for UV and visible cameras. However, as demands for these FPAs increase concomitantly with recent advances in material sciences, optics, and electronics, it is expected that newer and high-performance FPAs will be available in the near future not only with much lower cost but also with larger size, better performance, wider spectral response, and faster readout.

Depending on the spectral region, and even in the same region, there are many different types of IR FPAs. They include indium antimonide (InSb), platinum silicide (PtSi), indium gallium arsenide (InGaAs), germanium (Ge), mercury cadmium telluride (HgCdTe), and quantum well infrared photodetectors (QWIPs). In the following section, characteristics, advantages, and limitations of four of the most widely used IR FPAs in IR multispectral imaging, i.e., InGaAs, InSb, HgCdTe, and QWIP, will be described.

InGaAs Focal Plane Arrays

InGaAs/InP is a direct bandgap intrinsic detector that is primarily used for application requiring response in the near-IR region (from 0.9 to 1.7 μm) (Cohen and Olsen 1993; Barton, Cannata, and Petronio 2002; Kozlowski et al. 1997). Having low dark current and noise and the ability to operate at room temperature have increasingly made InGaAs the FPA of choice for short-wavelength IR (SWIR) detection. Detailed information of the standard $In_{0.53}Ga_{0.47}As/InP$ detector structure has been previously described (Cohen and Olsen 1993; Barton, Cannata, and Petronio 2002; Kozlowski et al. 1997). Current work has focused on extending cutoff wavelength to 2.6 μm. Highest performance, however, is best achieved when lattice matched at

cutoff wavelength of approximately 1.7 μm and grown via metal–organic chemical vapor deposition. InGaAs FPAs with large numbers of pixels (640 × 512) and high performance (128 × 128 InGaAs FPA with room-temperature D^* value of 1.5×10^{13} cm-Hz$^{1/2}$/W and D^* value at 195°K of 11.1×10^{15} cm-Hz$^{1/2}$/W for 1.0 to 1.7 μm range) are currently commercially available. By varying the indium content, InGaAs FPAs sensitive to 2.0 μm are now available in 320 × 240 format (Cohen and Olsen 1993; Barton, Cannata, and Petronio 2002).

As described in the following section and summarized in Table 2, detection of SWIR can also be achieved with FPAs based on InGaAs, InSb, or HgCdTe. Among the three, InGaAs and HgCdTe can be used at room temperature, whereas InSb must be cooled to about 80°K. Both InGaAs and HgCdTe can offer radiatively limited detector performance that translates to the higher possible D^*. InGaAs FPA may be the detector of choice, when cost is taken into account, and when longest detection wavelength is 1.7 μm (Cohen and Olsen 1993; Barton, Cannata, and Petronio 2002).

InSb Focal Plane Arrays

InSb is a semiconductor with a bandgap energy of 0.22 eV at 77°K, which is suitable for detection of IR radiation from 1 to 5 μm (Kimata 1998; Rogalski 2001; Kozlowski 1997; Gopal 1998; Faraone 1998). As a consequence, it is an equally sensitive alternative to HgCdTe for middle-wavelength IR (MWIR) applications. InSb is relatively easier to produce than HgCdTe; relatively large-diameter InSb wafers can be obtained from single crystal ingots. This capability extends the current InSb technology to larger FPAs than HgCdTe FPA, and thus, high-quality thermal images with large pixel areas are readily available. As a consequence, InSb is often the FPA of choice for high-sensitivity MWIR applications that require good, corrected uniformity (Kimata 1998; Rogalski 2001; Kozlowski 1997; Gopal 1998; Faraone 1998).

Table 2. Properties of different types of materials for infrared cameras

Material	Bandgap energy (eV)	Wavelength cutoff (μm)	Operating temperature (°K)
In$_x$GaAs/InP with $x = 0.53$	0.73	1.7	280
In$_x$GaAs/InP with $x = 0.80$	0.49	2.5	270
HgCdTe	Tunable	1 to ~18	50–250
InSb	0.18	6.89	80
QWIP	Tunable	Tunable	~40

Mercury Cadmium Telluride (HgCdTe) Focal Plane Arrays

HgCdTe (commonly pronounced "mer-cad-telluride") has been the dominant FPA for the IR region. This is due to the fact that the bandgap energy of $Hg_{1-x}Cd_xTe$ can be readily controlled by judiciously adjusting its composition. As a consequence, $Hg_{1-x}Cd_xTe$ FPAs cover all spectral bands from the SWIR (from 1 to 3 μm) to long-wavelength IR (LWIR) (from 6 to 12 μm). Traditionally, this type of FPA is produced from thin $Hg_{1-x}Cd_xTe$ layers epitaxially grown by liquid-phase epitaxy on closely lattice-matched CdTe or CdZnTe substrates (Gopal 1998; Faraone 1998). This technology offers the highest-quality epitaxial $Hg_{1-x}Cd_xTe$ layer so far. Its advantages include high sensitivity, ability to select cutoff wavelength at time of manufacture, and high operating temperature. Because of these advantages, HgCdTe often seems to be the FPA of choice for IR detection. In fact, HgCdTe FPAs can provide detection from 2 to 26 μm. However, large arrays have been built only to a cutoff of 10 or 11 μm. Operating HgCdTe at warmer temperatures naturally increases the thermally generated noise. The increased noise also manifests itself as a decrease in dynamic range. Compared to other types of IR FPAs, the biggest drawbacks with HgCdTe are its instability and nonuniformity problems over large areas due to high Hg vapor pressure during the material growth and problems associated with thermal expansion mismatch. This leads to high costs, delayed schedules, nonuniformity, and unfulfilled performance promises (Table 3). Furthermore, the problems magnify as cutoff wavelength increases (Gopal 1998; Faraone 1998).

Quantum Well Infrared Photodetectors (QWIP)

As described in the previous section, LWIR (8–12 μm) imaging systems traditionally have relied on HgCdTe as the only suitable FPA material. The advantages of HgCdTe FPAs are well-known: tunable cutoff wavelength, high quantum efficiency, and significantly higher operation temperature than many other long-wavelength detector materials. However, as described in the previous paragraph, there are problems associated with LWIR FPAs based on HgCdTe, including its instability and nonuniformity problems over large areas, and the difficulty in finding reliable production.

    Long-wavelength FPAs have also been developed utilizing superlattices or (multiple) quantum well infrared photodetectors (QWIP) (Gunapal et al. 2001). A quantum well technology can be used to construct a detector for a particular wavelength by designing the potential depth and width of the well to produce two states separated by the desired photon energy. A FPA based on quantum well can, therefore, be constructed from a compositional superlattice structure that is made from thin alternating layers of different semiconductors. The periodicity that the layer structure produces results in a change in band structure in the direction perpendicular to the layers and

Table 3. Advantages and disadvantages of infrared cameras

Detector type	Advantages	Disadvantages
InGaAs	Good material and dopants, advanced technology, high D^* values at room temperature	Limited detection range, difficult to produce uniform and high-performance arrays sensitive for wavelengths longer than 1.7 μm
III–V (InSb)	Good material and dopants, advanced technology, possible monolithic integration	Heteroepitaxy with large lattice mismatch
Quantum well infrared photodetector	Matured material growth, good uniformity over large area, multicolor detectors	Low quantum efficiency, complicated design and growth, limited range within a specifically designed material: not a broad spectral tuning range camera

produces subbands. Only photons having energies corresponding to the energies of the subbands are absorbed. These subbands can be tuned by varying the layer thickness. As a consequence, wavelength range detected by this type of FPA can be appropriately tuned. In fact, researchers at the Jet Propulsion Lab have recently developed a QWIP FPA by alternating layers of GaAs (the well material) and $Al_xGa_{1-x}As$ (the potential barrier) (Gunapal et al. 2001). The wavelength of light that the QWIP responds to can be chosen by varying the thickness of the layers and the mole fraction x in the $Al_xGa_{1-x}As$ layer (Gunapal et al. 2001). These layers are deposited by molecular beam epitaxy for precise control of QWIP characteristics. The $GaAs/Al_xGa_{1-x}As$ material system can be tweaked over a wide range to enable detection of light at wavelengths longer than 6 μm (Gunapal et al. 2001). Multispectral detection can be achieved by stacking QWIP chips having different bandgap superlattices and connecting them with multichannel readouts.

QWIP FPAs push the operating temperature from below 12°K to as high as 40°K, depending upon peak wavelength. However, they may have inadequate quantum efficiency to yield satisfactory D^*. In fact, D^* values of most QWIP FPAs are reportedly in the range 10^{10} to 10^{11} Jones at operating temperature of about 78°K. This is due to higher dark current and lower efficiency. Gunapal (2001) estimated that the highest possible D^* value of QWIP is about 10^{11}. HgCdTe FPAs, on the other hand, can have

D^* as high as 10^{14} and 10^{13} at 10 and 16 μm, respectively (Gopal 1998; Faraone 1998). However, QWIP FPAs can have the advantage when they are operated at lower temperature. For example, QWIP is known to have superior performance relative to HgCdTe at 45°K. Furthermore, HgCdTe FPAs with pixel yield greater than 99.5% cannot be consistently achieved (Gopal 1998; Faraone 1998).

APPLICATIONS

As described in the previous section, ATOFs offer such advantages as being compact, being all-solid state (contains no moving parts), having rapid scanning ability (microseconds), having wide spectral tuning range (from visible to NIR and IR), and having high throughput (>90% diffraction efficiency for incident polarized light), allowing high-speed random or sequential wavelength access, and giving high resolution (a few angstroms). As a consequence, ATOF provides not only the simplicity in construction of a multispectral imaging instrument but also ease of operation. Features such as high sensitivity, fast scanning speed made it possible for the AOTF-based imaging spectrometer to be used for studies that are not possible with other spectral tuning devices, such as the LCTFs or the interferometers (Tran, Cui, and Smirnov 1998; Fischer and Tran 1999a, 1999b; Tran 2000b, 2001; Khait, Smirnov, and Tran 2000, 2001; Alexander and Tran 2001a, 2001b; Politi and Tran 2002; Morris, Schaeberle, and Treado 1995; Turner and Treado 1997). For example, an AOTF-based imaging instrument was used successfully for the determination of inhomogeneity in the kinetics of curing of epoxy resins. It also shows that the initial hydrolysis and the subsequent condensation step of the solgel reaction processes are indeed inhomogeneous, and because of this kinetics inhomogeneity, the chemical distribution of the final product is inhomogeneous (Tran, Cui, and Smirnov 1998; Fischer and Tran 1999a, 1999b; Tran 2000b, 2001; Khait, Smirnov, and Tran 2000, 2001; Alexander and Tran 2001a, 2001b; Politi and Tran 2002). Of particular interest is the study of the molecular state and distribution of proteins encapsulated in a solgel sample (Politi and Tran 2002; Morris, Schaeberle, and Treado 1995; Turner and Treado 1997; Tran, Ilieva, and Challa 2004). By use of an AOTF-based imaging instrument, it was demonstrated that the encapsulated protein was distributed inhomogeneously throughout the solgel sample, and the conformations of the protein molecules are different (Tran, Ilieva, and Challa 2004).

An imaging instrument based on the AOTF is compact, contains no moving parts, and requires relatively low electrical power. As a consequence, it can be powered by a battery and, hence, is particularly suited for field measurements. In fact, an ATOF-based imaging instrument has been deployed for agricultural and environmental measurements directly in the

field (Inoue et al. 2001; Endo, Yasuoka, and Tamura 2001). It was used successfully for the determination of leaf nitrogen and chlorophyll contents of the rice canopies (Inoue et al. 2001; Endo, Yasuoka, and Tamura 2001). The same instrument was also used to record weak spectral images at 970 nm for the determination of water content of leaf. It was suggested that this imaging instrument could also be used to assess uptake of CO_2 gas by the canopy (Endo, Yasuoka, and Tamura 2001). The kinetics of water desorption from olive leaves was successfully determined using an AOTF-based imaging instrument. It was found that the water of water desorption is strongly dependent on the environment in which the leaves were stored (Tran and Grishko 2004). Water is desorbed from leaves faster when leaves are stored under dry conditions (Tran and Grishko 2004). The rate for leaves stored in 0% humidity is 1.5 times faster than those stored in 50% humidity. The detection of land mines and buried objects requires methods that can cover large areas rapidly while providing the required sensitivity to detect the optical and spectroscopic contrasts in soil properties that can reveal their presence (Mobley et al. 1999). It was reported recently that these conditions on contrast and coverage were met, and land mines and buried objects can be readily detected by use of the AOTF-based spectral imaging instrument to capture hyperspectral images (Mobley et al. 1999).

It is noteworthy to add that infrared multispectral imaging is not restricted to macroscopic imaging with spatial resolution of about 10 μm, such as that described in the previous paragraph. Microscopic imaging can be accomplished by incorporating a microscope into the imaging system. In fact, a NIR multispectral imaging microscopic instrument based on an AOTF has been constructed (Khait, Smirnov, and Tran 2000, 2001). In addition to its high spatial resolution (about 1 μm), because of the fast scanning characteristics of the AOTF, this microscopic imaging instrument has temporal resolution of a few milliseconds (Khait, Smirnov, and Tran 2000, 2001). It was successfully used, for the first time, to determine the spectral response of single-unit cells to a temperature-sensitive liquid crystal in millisecond time resolution (Khait, Smirnov, and Tran 2000, 2001). It was found that the unit cells distributed inhomogeneously throughout the liquid crystal, and each cell (about 1 μm in size) has different chemical, physical, and optical properties (Khait, Smirnov, and Tran 2000, 2001).

FUTURE PROSPECTS

Taken together, the advantages of the AOTF-based multispectral imaging instruments, including their instrumental simplicity, low cost, and superior performance (fast scan ability, high throughput), make them uniquely suited for applications that are not possible with other spectral imaging techniques. Currently, most AOTF-based imaging instruments operate in the near- and

middle-IR region (up to about 5 μm), because they are based on the use of AOTFs that were fabricated from TeO_2 crystal, and this crystal is transparent in the $0.35-5.00$ μm region (Table 1). This should not limit the applications of these imaging instruments, because spectroscopic imaging in the NIR region (up to about 3 μm) has been found to be particularly useful in most cases. This is because it is a well-known fact that measurements in this NIR region require no pretreatment of samples, are noninvasive, and are nondestructive. Furthermore, because spatial resolution of multispectral imaging instruments is known to be diffraction limited, it is expected that spatial resolution is better in the NIR region than in the middle- and far-IR regions.

Concomitant with the increase in applications of multispectral imaging techniques is the demand for imaging instruments with better performance in terms of sensitivity, detection range, scanning rate, and portability. Applications in the NIR region are expected to be increased substantially because of its advantages. In this region, InGaAs cameras are relatively more popular than InSb and HgCdTe cameras. This is because, in addition to its high sensitivity and low cost, an InGaAs camera can be operated at room temperature. Such a feature facilitates development of fully field-deployable NIR multispectral imaging instruments that are suitable for remote sensing and online monitoring. The first generation of commercially available InGaAs cameras are sensitive only from 1.0 to 1.7 μm. A new generation of InGaAs cameras with fast frame rate and wider spectral response have become commercially available recently. These cameras are equipped with 320×256 pixels and are sensitive not only in the NIR region (up to 1700 nm) but also in the visible region as well (down to 400 nm) (Ettenberg et al. 2002; Riboli, Saiani, and Gaburro 2004; Indigo Corporation 2004). It is anticipated that this visible-NIR range will greatly extend applications of the multispectral imaging techniques to many disciplines, including bioanalytical chemistry and agricultural remote sensing. Efforts have been made to extend the spectral response of the InGaAs cameras. It is anticipated that InGaAs FPAs sensitive up to 3 μm will be available soon. In fact, linear arrays InGaAs sensitive to 2.6 μm are currently commercially available, and InGaAs FPAs sensitive up to 2 μm have been reported (Ettenberg et al. 2002; Riboli, Saiani, and Gaburro 2004; Indigo Corporation 2004). Considerable advances on other FPAs have also been made. For example, it has been reported recently that a high-resolution NIR camera based on HgCdTe FPA equipped with 640×512 pixels with 18 μm pitch and broad spectral response (from 0.9 to 2.0 μm) with near 100% optical fill factor has been developed (Cabelli et al. 2003). The long-wavelength IR region (from 8 to 12 μm) is also of particular interest for field measurements and remote sensing, because it is immune to the solar flare. It is expected that spectroscopic measurements in this region will increase substantially in the near future because of important developments made recently, including an

AOTF based on Tl_3AsSe_3 that is capable of operating in the $8-12$ μm region (Suhre and Villa 1998), and the availability of high-performance and fast-frame-rate HgCdTe and QWIP cameras.

REFERENCES

Alexander, T., Gao, G.H., and Tran, C.D. 1997. Development of a novel fluorimeter based on superluminescent light emitting diodes and an acousto-optic tunable filter and its application in the determination of chlorophyll a and b. *Appl. Spectrosc.*, 51: 1603–1606.

Alexander, T. and Tran, C.D. 2001a. Near infrared spectrometric determination of di- and tripeptides synthesized by combinatorial solid phase method. *Anal. Chem.*, 73: 1062–1067.

Alexander, T. and Tran, C.D. 2001b. Near-infrared multispectral imaging technique for visualizing sequences of di- and tripeptides synthesized by solid phase combinatorial method. *Appl. Spectrosc.*, 55: 939–945.

Baptista, M.S., Tran, C.D., and Gao, G.H. 1996. Near infrared detection of flow injection analysis by acousto-optic tunable filter based spectrophotometry. *Anal. Chem.*, 68 (6): 971–976.

Barton, J.G., Cannata, R.F., and Petronio, S.M. 2002. InGaAs NIR focal plane arrays for imaging and DWDM applications. *Proc. SPIE*, 4721: 37–47.

Bhargava, R. and Levin, I.W. 2001. Fourier transform infrared imaging: Theory and practice. *Anal. Chem.*, 73: 5157–5167.

Cabelli, S.A., Pan, J., Bernd, S.G., Tennant, W.E., Blackwell, J.D., Bhargava, S., Pasko, J.G., Piquette, E.C., and Edwall, D.D. 2003. High resolution extended NIR camera. *Proc. SPIE*, 5074: 343–352.

Cohen, M.J. and Olsen, G.H. 1993. Room temperature InGaAs camera for near-IR imaging. *Proc. SPIE*, 1946: 436–443.

Colarusso, P., Didder, L.H., Levin, I.W., Fraser, J.C., Arens, J.F., and Levis, E.N. 1998. Infrared spectroscopic imaging: From planetary to cellular systems. *Appl. Spectrosc.*, 52: 106A–120A.

Endo, T., Yasuoka, Y., and Tamura, M. 2001. Spatial estimation of biochemical parameters for leaves with hyperspectral imager. *Proceedings, 22nd Asian Conference on Remote Sensing*, Asian Association on Remote Sensing (AARS), Eds.; Center for Remote Imaging, Sensing and Processing (CRISP), National University of Singapore; Singapore Institute of Surveyors and Valeurs (SI SV).

Ettenberg, M.H., Cohen, M.J., Brubaker, R.M., Lange, M.J., O'Grady, M.T., and Olsen, G.H. 2002. Indium gallium arsenide imaging with smaller cameras, higher resolution arrays and greater material sensitivity. *Proc. SPIE*, 4721: 26–36.

Faraone, L. 1998. HgCdTe infrared detector technology. In *Physics of Semiconductor Devices*; Kumar, V. and Agarwal, S.K., Eds.; Norosa Publishing House: India, 721–728.

Fischer, M. and Tran, C.D. 1999a. Evidence for kinetic inhomogeneity in the curing of epoxy using the near-infrared multispectral imaging technique. *Anal. Chem.*, 71: 953–959.

Fischer, M. and Tran, C.D. 1999b. Investigation of solid phase peptide synthesis by the near infrared multispectral imaging technique: A novel detection method for combinatorial chemistry. *Anal. Chem.*, 71: 2255–2261.

Gopal, V. 1998. Key issues of HgCdTe hybrid focal plane array technology. In *Physics of Semiconductor Devices*; Kumar, V. and Agarwal, S.K., Eds.; Norosa Publishing House: India, 729–737.

Gunapal, S., Bandara, S., Bock, J., Ressler, M., Liu, J., Mumolo, J., Rafol, S., Ting, D., and Werner, M. 2001. Large format long wavelength GaAs/AlGaAs multi-quantum well infrared detector arrays for astronomy. *Proc. SPIE*, 4288: 278–285.

Indigo Corporation. 2004, April. *News release*, Goleta, CA.

Inoue, Y., Penueleus, J., Nouevllon, Y., and Moran, M.S. 2001. Hyperspectral reflectance measurements for estimating eco-physiological status of plants. *Proc. SPIE*, 4151: 153–163.

Khait, O., Smirnov, S., and Tran, C.D. 2000. Time resolved multispectral imaging spectrometer. *Appl. Spectrosc.*, 54: 1734–1742.

Khait, O., Smirnov, S., and Tran, C.D. 2001. Multispectral imaging microscope with millisecond time resolution. *Anal. Chem.*, 73: 732–739.

Kimata, M. 1998. Infrared focal plane arrays. *Sensors Update*, 4: 53–79.

Kozlowski, L.J. 1997. HgCdTe focal plane arrays for high performance infrared cameras. *Proc. SPIE*, 3179: 200–211.

Kozlowski, L.J., Vural, K., Aria, J.M., Tennant, W.E., and DeWames, R.E. 1997. Performance of HgCdTe, InGaAs and quantum well GaAs/AlGaAs staring infrared focal plane arrays. *Proc. SPIE*, 3182: 2–13.

Lewis, E.N., Kidder, L.H., Arens, J.F., Peck, M.C., and Levin, I.W. 1997. Si:As focal plane array detection for fourier transform spectroscopic imaging in the infrared fingerprint region. *Appl. Spectrosc.*, 51: 563–567.

Lewis, E.N., Treado, P.J., Reeder, R.C., Story, G.M., Dewrey, A.E., Marcott, C., and Levin, I.W. 1995. Fourier transform spectroscopic imaging using an infrared focal plane array detector. *Anal. Chem.*, 67: 3377–3381.

Miller, P.J. 1991. Use of tunable crystal filters to link radiometric and photometric standards. *Metrologia*, 28: 145–149.

Miller, P.J. 1995. Multispectral imaging with liquid crystal tunable filter. *Proc. SPIE*, 2345: 354–365.

Mobley, J., Miller, G.H., Kasili, P.M., DiMarzio, C., and Vo-Dih, T. 1999. Hyperspectral imaging using AOTF and NIR sensing of buried objects and land mines. *Proc. SPIE*, 3534: 321–327.

Morris, H.R., Schaeberle, M.D., and Treado, P.J. 1995. Chemical imaging with tunable filters: Methods and applications. *Proc. SPIE*, 2385: 89–94.

Morris, M.D. 1993. *Microscopic and spectroscopic imaging of the chemical state*; Marcel Dekker: New York.

Pasquini, C., Lu, J., Tran, C.D., and Smirnov, S. 1996. Detection of flow injection analysis with pH gradient by acousto-optic tunable filter based spectrophotometry. *Anal. Chim. Acta*, 319: 315–324.

Politi, M. and Tran, C.D. 2002. Visualizing chemical compositions and kinetics of sol-gel by near-infrared multispectral imaging technique. *Anal. Chem.*, 74: 1604–1610.

Rafferty, D.W., Koenig, J.L., Magyar, G., and West, J.L. 2002. Fourier Transform infrared imaging of nematic liquid crystals. *Appl. Spectrosc.*, 56: 284–287.

Riboli, F., Saiani, M., and Gaburro, Z. 2004. Silicon-based near-infrared tunable filters based on liquid crystals. *Proc. SPIE*, 5357: 158–163.

Rogalski, A. 2001. Infrared detectors at the beginning of the next millennium. *Proc. SPIE*, 4413: 307–322.

Scott, W.H., Bhargava, R., and Levin, I.W. 2002. Generalized implementation of rapid scan Fourier transform infrared spectroscopic imaging. *Appl. Spectrosc.*, 56: 965–969.

Snively, C.M., Katzenberger, S., Oskarsdottir, G., and Lauterbach, J. 1999. Fourier transform infared imaging using a rapid scan spectrometer. *Opt. Lett.*, 24: 1841–1843.

Suhre, D.R. and Villa, E. 1998. Imaging spectroradiometer for the 8–12 μm region with a 3-cm^{-1} passband acousto-optic tunable filter.. *Appl Opt.*, 37: 2340–2345.

Tran, C.D. 1992. Acousto-optic devices: New optical elements for spectroscopy. *Anal. Chem.*, 64: 971A–981A.

Tran, C.D. 1995. Principles and analytical applications of acousto-optic tunable filters. *Anal. Sci. Technol.*, 8: 101A–108A.

Tran, C.D. 1997. Principles and analytical applications of acousto-optic tunable filters, an overview. *Talanta*, 45: 237–248.

Tran, C.D. 2000a. Acousto-optic tunable filter: A new generation monochromator and more. *Anal. Let.*, 33: 1711–1732.

Tran, C.D. 2000b. Visualizing chemical composition and reaction kinetics by near infrared multispectral imaging technique. *J. Near-Infrared Spectrosc.*, 8: 87–99.

Tran, C.D. 2001. Development and analytical applications of multispectral imaging techniques. *Fres. J. Anal. Chem.*, 369: 313–319.

Tran, C.D. and Bartelt, M. 1992. Performance characteristics of acousto-optic tunable filter for optical spectrometry. *Rev. Sci. Instrum.*, 63: 2932–2939.

Tran, C.D., Cui, Y., and Smirnov, S. 1998. Simultaneous multispectral imaging in the visible and near infrared region: Applications in document authentication and determination of chemical inhomogeneity of copolymers. *Anal. Chem.*, 70: 4701–4708.

Tran, C.D. and Furlan, R.J. 1992a. Electronic tuning, amplitude modulation of lasers by computer controlled acousto-optic tunable filter. *Appl. Spectrosc.*, 46: 1092–1095.

Tran, C.D. and Furlan, R.J. 1992b. Acousto-optic tunable filter as a polychromator and its application in multidimensional fluorescence spectrometry. *Anal. Chem.*, 64: 2775–2782.

Tran, C.D. and Furlan, R.J. 1993. Spectrofluorimeter based on acousto-optic tunable filters for rapid scanning and multicomponent sample analyses. *Anal. Chem.*, 65: 1675–1681.

Tran, C.D. and Furlan, R.J. 1994. Amplitude stabilization of a multiwavelength laser beam by an acousto-optic tunable filter. *Rev. Sci. Instrum.*, 65: 309–314.

Tran, C.D., Furlan, R.J., and Lu, J. 1994. Development of a multiwavelength thermal lens spectrophotometer based on an acousto-optic tunable filter as a polychromator. *Appl. Spectrosc.*, 48: 101–106.

Tran, C.D. and Gao, G.H. 1996. Characterization of an erbium doped fiber amplifier as a light source and development of a near-infrared spectrophotometer based on the EDFA and an acousto-optic tunable filter. *Anal. Chem.*, 68: 2264–2269.

Tran, C.D. and Gao, G.H. 1997. Determination of monomethylhydrazine with a novel, high throughput, all fiber near infrared spectrometer based on integrated acousto-optic tunable filter and erbium doped fiber amplifier. *Anal. Chem.*, 69: 1461–1465.

Tran, Chieu D. and Grishko, V. 2004. Determination of water contents in leaves by near-infrared multispectral imaging technique.. *Microchem J.*, 76: 91–94.

Tran, C.D. and Huang, G.C. 1999. Characterization of the collinear beam acousto-optic tunable filter (CB-AOTF) and its comparison with the noncollinear AOTF and the integrated AOTF. *Opt. Eng.*, 38: 1143–1148.

Tran, C.D. and Lu, J. 1995. Characterization of the acousto-optic tunable filter for the ultraviolet and visible regions and development of an AOTF-based rapid scanning detector for HPLC. *Anal. Chim. Acta.*, 314: 57–66.

Tran, C.D. and Lu, J. 1996. Detection of flow injection analysis by acousto-optic tunable filter based fluorimetry and its application in the determination of solvent polarity. *Appl. Spectrosc.*, 50: 1578–1584.

Tran, C.D. and Simianu, V. 1992. Multiwavelength thermal lens spectrophotometer based on acousto-optic tunable filter. *Anal. Chem.*, 64: 1419–1425.

Tran, C.D., Ilieva, D., and Challa, S. 2004. Inhomogeneity in distribution and conformation of bovine serum albumin in sol-gel: A closer look with a near-infrared multi-spectral imaging technique. *J. Sol-Gel Sci. Tech.*, 32: 1–11.

Turner, J.F. and Treado, P.J. 1997. LCTF Raman chemical imaging in the near-infrared. *Proc. SPIE*, 3061: 280–283.

Weerd, J.V., Brammer, H., Boon, J.J., and Heeren, R.M.A. 2002. Fourier transform infrared microscopic imaging of an embedded paint cross section. *Appl. Spectrosc.*, 56: 275–283.